

PAPER • OPEN ACCESS

Particle migration due to non-uniform laminar flow

To cite this article: M A Curt Koenders and Nick Petford 2024 *Fluid Dyn. Res.* **56** 055508

View the [article online](#) for updates and enhancements.

You may also like

- [Performance of Ag/La_{0.6}Sr_{0.4}Co_{1-x}Fe_xO₃ \(x = 0 - 0.8\) Nanotube Composite Cathodes for IT-SOFCs](#)
Martín G. Bellino, Joaquín G. Sacanell, Diego G. Lamas et al.
- [Differentiation of Enceladus and Retention of a Porous Core](#)
Wladimir Neumann and Antonio Kruse
- [NiO/ZrO₂-CeO₂ Anodes for Single-Chamber Solid-Oxide Fuel Cells Operating on Methane/Air Mixtures](#)
Diego G. Lamas, Marcelo D. Cabezas, Ismael O. Fábregas et al.

Particle migration due to non-uniform laminar flow

M A Curt Koenders^{1,*} and Nick Petford²

¹ Infrastructure Research Group, Department of Civil, Maritime and Environmental Engineering, Faculty of Engineering and Physical Sciences, Boldrewood Innovation Campus, University of Southampton, Southampton SO16 7QF, United Kingdom

² Department of Earth Sciences, Durham Energy Institute, Durham University, South Road, Durham DH1 3LE, United Kingdom

E-mail: mak2c08@soton.ac.uk and nick.petford@durham.ac.uk

Received 12 March 2024; revised 12 August 2024

Accepted for publication 7 October 2024

Published 22 October 2024

Communicated by Professor Dr Martin Oberlack



CrossMark

Abstract

Using methods of granular mechanics in the quasi-static limit, with inter-particle interactions derived from the lubrication limit, the intensity of velocity fluctuations in the slurry is associated with fluctuations in the local distribution of inter-particle distances. These are shown to consist of a vector intensity and a scalar intensity; the former couples to the first velocity gradient, the latter (which is associated with solidosity fluctuations) couples to the second velocity gradient. Rheologies for both are presented, as is the rheology that links the particle pressure to the intensity of the velocity fluctuations (also known as the ‘granular temperature’) to the dispersive pressure. The rheologies are informed by experimental results. The granular temperature profile, modified from previous work, is responsible for axial particle migration (Bagnold effect). Two broad categories are assessed: symmetrical vertical and non-symmetrical lateral flow. For the latter the roughness of the boundary walls and a non-zero density contrast are important; this case is studied for a system in which flow effects are confined to the immediate vicinity of the boundary. Sensitivity analysis reveals several key variables including the parameters that control a slipping boundary condition and the mean solidosity in the conduit. For lateral

* Author to whom any correspondence should be addressed.



Original Content from this work may be used under the terms of the [Creative Commons Attribution 4.0 licence](https://creativecommons.org/licenses/by/4.0/). Any further distribution of this work must maintain attribution to the author(s) and the title of the work, journal citation and DOI.

flow, a sedimentary deposit with a solidosity profile may develop near the upper or lower boundary. The theory predicts an approximate relation between the fluid-particle density contrast and sediment thickness as a function of the mean flow rate, conduit width, the mean particle diameter and fluid viscosity that has utility in a range of engineering and geological situations where particulate matter is transported in the laminar flow regime.

Keywords: suspension flow, particle migration, fluctuations

1. Introduction

Dense, slow slurry flow is of interest for applications in various branches of engineering, geology and materials science, and as a phenomenon in its own right as a sub-discipline of fluid mechanics. The literature is extensive and a full survey of all these fields and its many applications are beyond the scope of this article. The focus here is to present a first-order approximation of the key characteristics of suspension flows that seeks to better describe particle migration in congested mixtures of this type.

A simple delineation of the characteristics of these particle-fluid mixture flows is useful and it is important to distinguish regimes. The first parameter to consider is the mean particle size. For very small particles both Brownian motion and colloidal (double layer) interactions are important, as much as the flow properties, so particle size must be specified, both the mean diameter d as well as possibly a few numbers to characterise the grainsize distribution. Furthermore, something needs to be known about the particle shape, spherical, elliptical or otherwise. It may also be useful to obtain an impression of the surface roughness. The solids concentration properties need to be considered. This is most easily done by stating, in the first instance, the mean solids volume fraction ϕ (referred to in the chemical engineering literature as the solidosity). A further feature to consider in the context of applications in which gravity plays a prominent role, is the mass densities of the particles ρ_s and that of the fluid ρ_f .

All in all quite a few parameters describe the flowing motion and now it becomes clear why giving a summary of the literature is so difficult, because each application has its own typical parametric regime, thus revealing that what is appropriate for one application may be entirely irrelevant to another one. The subject has been of intense interest in the fluid dynamics literature and an extensive and informative review paper by Guazzelli and Pouliquen (2018) is referenced here.

Another issue is that in many applications the flows are sufficiently captured by a phenomenological approach. The underlying physics of the flow phenomena is not deemed to be relevant, or—if known—not easily applied to the particular process of interest. Physical modelling insight of fundamentals of processes is most easily obtained under simplified assumptions, so generally theories concern themselves with approximately spherical, mono-sized particles that all have the same mass density in elementary flow conditions, simple shear or pipe flow, for example. Size segregation of mixtures of particles in a fluid takes place, of course, but it is an added, albeit interesting, complication.

A feature of dense ($\phi > 0.2$, say) particle-fluid mixture flow in cases where there is a shear velocity gradient, such as in channel flow or Couette flow, is the emergence of a concentration profile; particles tend to migrate towards the region of low shear. The effect has been observed both in experiments (Bhattacharji 1967, Frank *et al* 2003) and in numerical simulations (Nott and Brady 1994). Similar features are also reported in geological field studies where magma (a high temperature suspension) has frozen rapidly in narrow conduits, preserving a concentration

profile consistent with inwards particle migration during flow: Gibb (1968), Komar (1972), Allgood *et al* (2024).

In numerical simulations the ambient conditions can be controlled very accurately and all particle-particle interaction effects can be switched off, so a purely fluid mechanical explanation is required. Also, the migration effect diminishes when Brownian motion, either real or introduced numerically, is present, see Frank *et al* (2003) and Koenders *et al* (2012). This is a first indication that the emergence of a concentration profile is associated with *fluctuations* in the particle motion. In a dense slurry particles must make excursions about their mean path motion in order to avoid one another, which introduces the irregular paths. When Brownian motion is introduced, extra fluctuations are added and these swamp the position-dependent shear-induced ones: the concentration profile disappears. In this paper the emphasis will be on particles that are large enough for Brownian motion to be irrelevant. The properties of the particle-particle interactions is going to be determined by hydrodynamic considerations in the first instance; these will be augmented with a phenomenological addition to capture the physics when particles are in very close proximity. The issue here is that in reality particles are never going to be exact mathematical spheres, but will always exhibit some form of roughness. Therefore, when particles come so close that their surfaces are within the roughness dimension, hydrodynamics is unable to capture exactly what takes place. This aspect of the problem has been treated in Jenkins and Koenders (2005), in which the surfaces of the particles are viewed as permeable porous media, thus avoiding the singularity that would appear in the fluid dynamics if surfaces were perfectly smooth.

Traditional models to describe the appearance of the concentration profile have concerned themselves with *diffusive models*. These are reported in the fluid dynamics literature, for example Leighton and Acrivos (1987), Phillips *et al* (1992), Miller and Morris (2006). In these papers the necessity of a collisional mechanism is identified; this in addition to a purely hydrodynamic interaction. Scaling arguments are put forward to come up with estimates of the diffusion coefficient. These models rely explicitly on the existence of a shear (or, equivalently, viscosity) gradient, which is slightly unsatisfactory for the following reason: where migration takes place in a situation in which there is an external source of fluctuation, for example in a vibrated system, the mean motion is zero, the shear gradient is zero and so these models predict no migration. Experiments, however—for example in oscillated filtration, Gundogdu *et al* (2003)—show a pronounced concentration profile, the shape and extent of which can be influenced by varying the vibration intensity. While it may be possible to adapt the diffusive models to replace the shear flow gradient aspect with an external agitation, it is better to use a model that makes explicit use of a measure of the velocity fluctuations that capture the nature of the origin of the migration. One such model is the *granular temperature model* by McTigue and Jenkins (1992).

The granular temperature model was much influenced by existing models on dry granular flow. In these, in addition to stress and strain fields, a temperature field is introduced, which is a measure for the quadratic velocity fluctuations. The temperature is a field parameter and therefore an extra balance equation is required and—again inspired by dry granular flow models—the one put forward is the *rate of working balance*. The problem with the model is that it has quite a large number of coefficients. McTigue and Jenkin's original idea was to derive these constants from a kinetic theory approach, much like molecular kinetic theories—see Chapman and Cowling (1970). The approach certainly gives answers. However, the accuracy of these must be questioned, as will be seen below. Essentially, for channel flow in which the particle diameter is much smaller than the conduit width, an extremely narrow solids concentration profile is predicted, which—alas—has not been found in either physical experiments—Frank

et al (2003)—or in numerical simulations—Koh *et al* (1994), Nott and Brady (1994), Lyon and Leal (1998), Koenders *et al* (2012).

Davis *et al* (2008), derive the constants of the granular temperature theory with a rate of working balance from a cell model. That approach also gives answers; these are very similar to the ones that follow from the kinetic theory approach and therefore have the same drawback. The problem is predominantly due to the implementation of the rate of working balance. Mixing the concepts of calorific heat and ‘granular heat’ may be neither straightforward, nor appropriate. Generally speaking, energy balances are very hard to get right in a granular mechanics context: Houlsby (1981), Dean (2015) and Koenders (2020) have shown that even simple stress–strain rate behaviour can only be obtained when fluctuations are taken into account; that is simply a fundamental property of a granular packing. It is thus well-worth looking at this issue in some depth.

Despite the difficulties with the constants in the granular temperature model—either derived from a kinetic theory or from a cell model—certain concepts are physically well-justified and worth preserving. The key issue is the concept of a *particle pressure*. While there is general acceptance of this concept—see Guazzelli and Pouliquen (2018)—a particular form was introduced by McTigue and Jenkins (1992) and set to be proportional to the square root of the granular temperature (that is, the quadratic velocity fluctuations). This same concept is employed in the cell model by Davis *et al* (2008). The question is then how to arrive at a reliable measure for this parameter. Deriving these constants from a cell model produces a ratio of the temperature T and its second derivative that is of the order of magnitude of $(d/W)^2$ (W is the macroscopic length scale of the problem). The cell model is obviously unable to provide information much beyond the size of the cell. Given such a ratio of length scales it is clear that the result must be a concentration of solids of the order of magnitude of d/W , which—as noted above—is clearly *not* measured in either physical or numerical experiments in conduit flow. A physically more realistic model should be able to incorporate a length scale that is something of the order of magnitude of the conduit width itself. While this is obvious, it must be remembered that the fluctuations are generated on the cell scale, as they are due to particles in dense shear flow necessarily evading one another due to their finite size and, associated with the roughness of the surfaces, colliding with one another. Therefore, the challenge is to devise a model that somehow combines the conduit scale flow properties with the local generation of velocity fluctuations. Guazzelli and Pouliquen (2018) also identify a non-local element that needs to be introduced into the theory.

Given the problems that come to the fore in the existing approaches to the migration problem, a new theory is put forward. The element of a particle pressure that is associated with the velocity fluctuation intensity, as proposed in the granular temperature theory, has been preserved. However, the velocity fluctuations are now obtained from the quasi-static force equilibrium of the particles. It turns out that they can be related to the fabric fluctuations intensity in the particle–fluid mixture. As mentioned above, these must exist, because particles in a dense sheared slurry make excursions from their mean flow paths. It transpires that the velocity fluctuations are associated not only with the *first gradient* of the flow, but also with the *second gradient*. The link with the first gradient couples to a vector-type fabric fluctuation property, while the link with the second gradient exhibits a scalar-type. Rheologies for these two fabric fluctuations intensities are put forward; they are informed by experiments and also a bit of physical intuition. Now, it becomes possible to obtain a particle pressure in terms of the first and second gradient of the flow field. For flow in a conduit this has the advantage that in regions where the first gradient (the shear) vanishes, there is still a finite particle pressure, because in these regions the second gradient does not vanish. So, the ugly singularity in the solidosity

profile that is a feature of the shear diffusion theories is removed. At the same time the difficulties with the scales of the granular temperature theory are alleviated, because no boundary value problem that involves the temperature needs to be solved. The second gradient provides a somewhat non-local element to the theory.

The theory, so derived is applied to conduit flow and also to flow of a thin layer of solids near a boundary. For the latter it is necessary to invoke slipping boundary conditions in both the velocity and the temperature.

2. The granular temperature model and the cell model

For dense, dry granular flows the granular temperature theory is a well established tool, Jenkins and Savage (1983), that has been extensively verified, both experimentally and in numerical simulations: Delannay *et al* (2007), Carlo *et al* (2019), Li *et al* (2024). The interactions in this case are collisional and frictional. The temperature is obtained from the fluctuations in the velocities of the particles, similar to the manner in which it is treated in the kinetic theory of gases, Chapman and Cowling (1970).

To adapt the theory to a fluid environment the dry version has been modified. The interaction is now the lubrication interaction. In dense flows the fluid merely serves as the interactive medium and—in a first approach—it is sufficient to treat the motion of the solid phase only.

2.1. Basic equations

The traditional balance equations of continuum mechanics apply (Becker and Buerger 1975). The quasi-static limit is applied. The rate of momentum balance equations for a mixture of incompressible particles and fluid in the quasi-static limit are (Drew 1986)

$$\frac{\partial(\phi \Sigma_{ij})}{\partial x_j} + \phi \rho_s g_i + \phi R(\phi)(U_i - v_i) = 0 \quad (1)$$

$$\frac{\partial[(1-\phi)\sigma_{ij}]}{\partial x_j} + (1-\phi)\rho_f g_i - \phi R(\phi)(U_i - v_i) = 0. \quad (2)$$

Here, ρ_s and ρ_f are the solid and fluid mass densities, ϕ is the particle volume fraction, Σ_{ij} and σ_{ij} are the components of the particle and fluid phase stresses, \mathbf{U} and \mathbf{v} the fluid and particle phase velocities, \mathbf{g} the gravitational acceleration and $R(\phi)$ the drag coefficient. Einstein's summation convention is used throughout. Adding the two equations together removes the drag term

$$\frac{\partial(\phi \Sigma_{ij})}{\partial x_j} + \frac{\partial[(1-\phi)\sigma_{ij}]}{\partial x_j} + \phi \rho_s g_i + (1-\phi)\rho_f g_i = 0. \quad (3)$$

The dominant contribution for the fluid stress is the pressure P , $\sigma_{ij} = -P\delta_{ij}$. The intergranular stress, that is the stress that represents the actual force between the particles, \mathbf{t} , is $t_{ij} = \phi \Sigma_{ij} + \phi P\delta_{ij}$. Using these then gives

$$-\frac{\partial P}{\partial x_i} + \rho_f g_i + \frac{\partial t_{ij}}{\partial x_j} + \phi(\rho_s - \rho_f)g_i = 0. \quad (4)$$

The fluid pressure contains a hydrostatic part $-\rho_f g_i x_i$ and an external pressure part p : $P = -\rho_f g_i x_i + p$, so in terms of the latter it is seen that

$$-\frac{\partial p}{\partial x_i} + \frac{\partial t_{ij}}{\partial x_j} + \phi(\rho_s - \rho_f)g_i = 0. \quad (5)$$

The way McTigue and Jenkins (1992) initially conceived the granular temperature model is as follows.

The static equation of continuity for the particulate phase is

$$\frac{\partial(\phi v_i)}{\partial x_i} = 0. \quad (6)$$

In the granular temperature model the fluctuations in the particle velocities are treated as heat motion; it then puts forward a correspondence between the theory of gases—Chapman and Cowling (1970)—(where the velocity fluctuations are due to actual heat motion) and a similar theory relevant to dry dilute particle flow (Jenkins and Savage 1983). The balance equation for the fluctuational energy content takes the form

$$-\frac{\partial Q_k}{\partial x_k} + t_{ik} \frac{\partial v_i}{\partial x_k} - \bar{\gamma} = 0 \quad (7)$$

where \mathbf{Q} is the granular heat flux and $\bar{\gamma}$ the rate of dissipation. The heat flux, Q is related to the temperature gradient by Fourier's law.

These are the balance equations for quasi-static situations. The cell model by Davis *et al* (2008), uses the same equations; they are essentially at the basis of continuum theory (Becker and Buerger 1975).

2.2. Constitutive equations

In addition to the balance equations constitutive laws are required. These naturally need constitutive constants. First of all the stress constitutive equation is put forward as a simple isotropic form in terms of the strain rate tensor $\dot{\mathbf{d}}$

$$t_{ik} = \bar{\lambda} \dot{d}_{kk} \delta_{ik} + 2\bar{\mu} \dot{d}_{ik} \quad (8)$$

where $\bar{\lambda}$ and $\bar{\mu}$ are the bulk and shear viscosities.

The full stress tensor requires a *particle pressure*. This parameter is taken to depend on the velocity fluctuations in the lubrication limit; McTigue and Jenkins (1992) and Davis *et al* (2008) put forward the following expression

$$\bar{p} = \alpha_4 \frac{\eta}{d} \phi \frac{d}{h} \sqrt{T}. \quad (9)$$

Here α_4 is a constitutive constant, η the fluid viscosity and h the mean surface-to-surface distance between the particles, which enters the lubrication limit via the ratio d/h . Below this expression will be analysed further.

In essence a particle pressure exists in those cases where the approach and departure of a particle pair is not along entirely reversible trajectories. When the particles are perfectly smooth reversibility may be the case and $\alpha_4 = 0$; $\alpha_4 \neq 0$ occurs when there is a non-viscous element. Such a case may arise when particles are rough, which has implications for the lubrication interaction. A non-viscous element may also arise when the particles are not perfectly rigid. In the suspension simulation community both roughness and non-rigidity have been invoked to avoid the singularity posed by the lubrication limit for $h \rightarrow 0$, see for example Seto and Giusteri (2018). Surface roughness, which could lead to a contact encounter between particles has been studied (Jenkins and Koenders 2005), and if a roughness dimension δ_r on the surfaces is introduced then the interaction does not behave according to the lubrication limit \dot{h}/h , but rather as $\dot{h}/(h + \delta_r)$. What this implies is that on approach particles touch when their surfaces come within a range of δ_r at relative velocity \dot{h}/δ_r . The collision is inelastic and so the relative velocity collapses to zero. On release the particles depart at relative velocity

zero; this is an irreversible process and makes $\alpha_4 \neq 0$. The non-rigidity aspect can be understood when a contact interaction is considered along Hertzian lines. The interaction with an indentation of magnitude h_c due to a contact force F_c has the form $F_c \propto h_c^{3/2}$. Now, the incremental stiffness is $\partial F_c / \partial h_c \propto h_c^{1/2}$, which vanishes for zero indentation $h_c \rightarrow 0$ and therefore the particle surface is soft. So elastic effects are possible when two particles come very close together. Whichever effect takes place, contact or near-contact events are associated with a particle pressure—purely hydraulic considerations are inadequate.

Estimates of the moduli $\bar{\mu}$ and $\bar{\lambda}$ are required and, again in the lubrication limit in which particles are close together, following McTigue and Jenkins (1992), these are proportional to the fluid viscosity η and take the form

$$\bar{\lambda} = \alpha_0 \eta \phi \frac{d}{h}; \quad \bar{\mu} = \alpha_1 \eta \phi \frac{d}{h}. \quad (10)$$

The constitutive relations required for the balance equation for the fluctuation content, equation (7), are more problematic. A way forward is proposed in the cell model (Davis *et al* 2008). However, the results are not relevant to problems in which the length scale of the problem is much greater than the particle diameter, as explained in the previous section. Therefore, this will not be pursued here any further.

The theory is essentially isotropic (refinements to include anisotropic features are possible). The coefficients α_{0-4} may then still depend on the volume fraction ϕ . In the theory the fluid plays the role of a mediator of the forces between the particles. The fluid motion is not treated separately.

2.3. Force balance analysis

Neither the cell model nor the kinetic theory address the question of time-dependence. In a quasi-static context this is quite easily introduced, as at all times the sum of forces on a given particle vanishes. To see how this works a notation (first developed for granular mechanics) is adopted as follows Koenders (2020): particles are numbered and they are identified by a Greek superscript; two superscripts are used to denote relations between particles. For example, particle μ will have position \mathbf{x}^μ and the branch vector $\mathbf{c}^{\mu\nu} = \mathbf{x}^\nu - \mathbf{x}^\mu$. The force exerted on particle μ by particle ν is $\mathbf{F}^{\mu\nu}$. The latter is approximated in the lubrication limit as, see Jenkins and Koenders (2005)

$$F_i^{\mu\nu} = \frac{3\pi}{8} \eta d \left(\frac{d}{h^{\mu\nu}} \right) (v_j^\nu - v_j^\mu) n_j^{\mu\nu} n_i^{\mu\nu} \quad (11)$$

where η is the fluid viscosity, $\mathbf{n}^{\mu\nu}$ the unit vector of the branch vector: $\mathbf{n}^{\mu\nu} = \mathbf{c}^{\mu\nu} / |\mathbf{c}^{\mu\nu}|$ and $h^{\mu\nu}$ the surface-to-surface distance between the two particles μ and ν . Expression (11) represents the first order term in d/h ; the next term is of the order $\log d/h$, see for example Kim and Karilla (1991).

The time-dependent element is introduced by making d/h a function of time. It is not known what the precise form of this function is. However, averages and variances can be used as parameters.

In passing it is noted that for most realistic cases—especially in geophysical applications—there will be substantial shape variability and grain size distributions are likely to be heterogeneous. Therefore, the theoretical analysis presented here is deficient in many aspects, but the aim of this paper is to establish the structure of the theory and all particles will be assumed to

be equal-sized, spherical ones. Shape and size variability can be introduced as refinements at a later stage.

2.3.1. Averages. Averaging over time and a small group of N^a nearby particles of a physical parameter Π is denoted by $\langle \Pi \rangle$ and defined as

$$\langle \Pi \rangle = \frac{1}{\tau N^a} \sum_{\lambda} \int_0^{\tau} \Pi^{\lambda}(t) dt. \quad (12)$$

For the ‘measurement time’ τ a suitable value is chosen, something of the order of $\bar{m}/|\partial \mathbf{v}/\partial \mathbf{x}|$, where \bar{m} is a large enough number to give sufficient time for particles to move past one another, but so small that only a few participating neighbouring particles need to be included. The particles participating in the averaging process are a central particle and its immediate neighbours. The average is therefore determined in a position defined by the central particle. One average that is troublesome is $\langle d/h \rangle$, which is very ill-defined due to the fact that pairs may touch. Instead the average $\langle h/d \rangle$ is used, which will be called s . The first estimate of d/h is thus $1/s$. Using this average a smooth, position-dependent parameter is possible. Fluctuations are time-dependent and denoted by a prime, so for example $h^{\mu\nu} = \langle h \rangle^{\mu} + h'^{\mu\nu}$.

2.3.2. Approximating the force balance. The sum of forces on a given particle μ due to N_c near-neighbours vanishes

$$F_i^e + \sum_{\nu=1}^{N_c} F_i^{\mu\nu} = 0. \quad (13)$$

Here an external force \mathbf{F}^e is given, which may be due to a fluid pressure gradient or a gravitational contribution. It is assumed to be either a constant, or only varying in a secular manner, that is, over a time scale that is long compared to τ . The idea is to insert (11) into the sum of forces and to that end the velocity of the particles is split in a secular and a fluctuating part, the latter is denoted by a prime; the secular part is expanded in a Taylor series

$$v_j^{\nu}(t) - v_j^{\mu}(t) = \left\langle \frac{\partial v_j}{\partial x_k} \right\rangle c_k^{\mu\nu} + \frac{1}{2} \left\langle \frac{\partial^2 v_j}{\partial x_k \partial x_l} \right\rangle c_k^{\mu\nu} c_l^{\mu\nu} + v_j^{\nu}(t) - v_j^{\mu}(t). \quad (14)$$

Similarly, d/h is split in a constant (or secular) and fluctuating part. Furthermore, the surface-to-surface distance may have a systematic part that is position-dependent; in order to accommodate that a first order Taylor series is used: $d/h^{\mu\nu} = (s^{\mu})^{-1} + 1/2 c_i^{\mu\nu} \langle \partial (s^{\mu})^{-1} \partial x_i \rangle^{\mu} + (\partial(d/h)/\partial h)^{\mu} h'^{\mu\nu}$; the single superscript μ is necessary to indicate that the time average and its derivative has been taken at the location of particle μ . The factor 1/2 in front of the gradient is necessary, because the distance between particles is evaluated half-way between them. $(\partial(d/h)/\partial h)^{\mu}$ is easily identified as $-d^{-1}(d^2/h^2)^{\mu} = -d^{-1}(s^{\mu})^{-2}$.

For notational convenience, in what follows, the averages of the components of the single and double velocity gradients are abbreviated as α_{jk} and α_{jkl} . The expansions for the velocity difference and the surface-to-surface distance are inserted into (11) and then equation (13) looks as follows (a superscript μ has been applied in order to make clear that these are strictly

local variables, evaluated in \mathbf{x}^μ)

$$\begin{aligned}
& \frac{8F^e_i}{\pi\eta d} + \sum_{\nu=1}^{N_c} \left[(s^\mu)^{-1} \alpha_{jk}^\mu c_k^{\mu\nu} + \frac{1}{2} \left[\left\langle \frac{\partial s^{-1}}{\partial x_l} \right\rangle^\mu \alpha_{jk}^\mu + (s^\mu)^{-1} \alpha_{jkl}^\mu \right] c_k^{\mu\nu} c_l^{\mu\nu} \right] n_j^{\mu\nu} n_i^{\mu\nu} \\
& + \frac{1}{4} \sum_{\nu=1}^{N_c} \left[\left\langle \frac{\partial s^{-1}}{\partial x_l} \right\rangle^\mu \alpha_{jkm}^\mu c_k^{\mu\nu} c_l^{\mu\nu} c_m^{\mu\nu} - \frac{1}{d} (s^\mu)^{-2} h'^{\mu\nu} \left(\alpha_{jk}^\mu c_k^{\mu\nu} + \frac{1}{2} \alpha_{jkl}^\mu c_k^{\mu\nu} c_l^{\mu\nu} \right) \right] n_j^{\mu\nu} n_i^{\mu\nu} \\
& \sum_{\nu=1}^{N_c} \left[(s^\mu)^{-1} + \frac{1}{2} c_l^{\mu\nu} \left\langle \frac{\partial s^{-1}}{\partial x_l} \right\rangle^\mu \right] [(v'_j)^\nu - (v'_j)^\mu] n_j^{\mu\nu} n_i^{\mu\nu} \\
& - \frac{1}{d} \sum_{\nu=1}^{N_c} (s^\mu)^{-2} h'^{\mu\nu} [(v'_j)^\nu - (v'_j)^\mu] n_j^{\mu\nu} n_i^{\mu\nu} = 0. \tag{15}
\end{aligned}$$

The equation is approximated to preserve only lowest and first order terms in the fluctuations; furthermore the sum over neighbouring particles—the ones labelled ν —of the velocity fluctuations is neglected and regarded as a higher order term.

The focus is now on the ‘structural sums’. These are sums over strings of branch vectors. In an average packing, with neighbours more or less uniformly (or at least symmetrically) distributed over the solid angle, the sum over an odd number will be much smaller than the sum over an even one. Using the methodology described by Davis *et al* (2008), the average values of these sums may be found by replacing the sum with an integral over a solid angle with a weight equal to $N_c/(4\pi)$. Thus,

$$\sum_{\nu=1}^{N_c} n_j^{\mu\nu} n_i^{\mu\nu} \approx \frac{N_c}{4\pi} \int_{\text{unit sphere}} n_i n_j d\Omega = \frac{N_c}{3} \delta_{ij} \tag{16}$$

$$\sum_{\nu=1}^{N_c} n_j^{\mu\nu} n_i^{\mu\nu} n_l^{\mu\nu} \approx 0 \tag{17}$$

$$\sum_{\nu=1}^{N_c} n_i^{\mu\nu} n_j^{\mu\nu} n_k^{\mu\nu} n_l^{\mu\nu} \approx \frac{N_c}{4\pi} \int_{\text{unit sphere}} n_i n_j n_k n_l d\Omega = \frac{N_c}{15} (\delta_{ij}\delta_{kl} + \delta_{il}\delta_{kj} + \delta_{ik}\delta_{jl}). \tag{18}$$

Using this equation (15) reduces to

$$\begin{aligned}
& -v_i^\mu (s^\mu)^{-1} \frac{N_c}{3} - \frac{1}{d(s^\mu)^2} \sum_{\nu=1}^{N_c} h'^{\mu\nu} c_k^{\mu\nu} n_j^{\mu\nu} n_i^{\mu\nu} \alpha_{jk}^\mu - \frac{1}{d(s^\mu)^2} \sum_{\nu=1}^{N_c} h'^{\mu\nu} c_k^{\mu\nu} c_l^{\mu\nu} n_j^{\mu\nu} n_i^{\mu\nu} \alpha_{jkl}^\mu \\
& + \frac{N_c}{30} (\delta_{ij}\delta_{kl} + \delta_{il}\delta_{kj} + \delta_{ik}\delta_{jl}) \left[(s^\mu)^{-1} \alpha_{jkl}^\mu + \left(\frac{\partial s^{-1}}{\partial x_l} \right)^\mu \alpha_{jk} \right] + \frac{8}{3\pi\eta d} F^e_i = 0. \tag{19}
\end{aligned}$$

Approximating $h \ll d$, so that $|\mathbf{c}| \approx d$ leaves the lowest order terms only

$$\frac{3\pi\eta d^3 N_c}{80} (\delta_{ij}\delta_{kl} + \delta_{il}\delta_{kj} + \delta_{ik}\delta_{jl}) \left[(s^\mu)^{-1} \alpha_{jkl}^\mu + \left(\frac{\partial s^{-1}}{\partial x_l} \right)^\mu \alpha_{jk} \right] + F^e_i = 0. \tag{20}$$

It is easy to recognise the stress equilibrium—equation (5)—here, where there is a viscosity tensor \mathbf{A} . To that end the external force is derived from a pressure gradient (possibly including

a gravity term). The pressure comes from two contributions, a fluid pressure p and a particle pressure \bar{p} . The force on a particle with surface area A_p and volume V_p is then

$$F_i^e = - \int_{A_p} (p + \bar{p}) n_i dA + \int_{V_p} (\rho_s - \rho_m) g_i dV. \quad (21)$$

Using Gauss' theorem the first integral may be recast in a volume integral and \mathbf{F}^e becomes

$$F_i^e = \int_{V_p} \left(-\frac{\partial(p + \bar{p})}{\partial x_i} + (\rho_s - \rho_m) g_i \right) dV \rightarrow V_p \left(-\frac{\partial(p + \bar{p})}{\partial x_i} + (\rho_s - \rho_m) g_i \right) \quad (22)$$

where $V_p = \pi d^3/6$.

The viscosity tensor is defined such that the link between the pressure gradient and the strain rate \mathbf{d} is $(\partial p/\partial x_i) = \partial(A_{ijkl} \dot{d}_{kl})/\partial x_j$; the strain rate is $\dot{d}_{kl} = 1/2(\partial v_k/\partial x_l + \partial v_l/\partial x_k)$. Sweeping it all together then

$$A_{ijkl}^\mu = \frac{9\eta N_c}{40} (s^\mu)^{-1} (\delta_{ij}\delta_{kl} + \delta_{il}\delta_{kj} + \delta_{ik}\delta_{jl}). \quad (23)$$

Given the pressure gradient, the solidosity profile, the profile of $\langle d/h \rangle$ and boundary conditions these low order results can be used to determine the velocity, velocity gradient and double gradient.

An alternative route to the viscosity tensor is to impose the viscous rheology on the stress tensor \mathbf{t} ; the latter may be derived from the first moment of the interactive force. This was first derived, based on quasi-static equilibrium, by Love (1934) and subsequently much used in granular mechanics publications, see Koenders (2020) for details. Both the method to get to (23), as done here, or Love's elegant approach are based on equilibrium and thus equivalent.

Now turning to the fluctuations in equation (19), an equation is left to determine the velocity fluctuations

$$v_i'^{\mu} (s^\mu)^{-1} \frac{N_c}{3} + \frac{1}{d(s^\mu)^2} \sum_{\nu=1}^{N_c} h'^{\mu\nu} c_k^{\mu\nu} n_j^{\mu\nu} n_i^{\mu\nu} \alpha_{jk}^\mu + \frac{1}{d(s^\mu)^2} \sum_{\nu=1}^{N_c} h'^{\mu\nu} c_k^{\mu\nu} c_l^{\mu\nu} n_j^{\mu\nu} n_i^{\mu\nu} \alpha_{jkl}^\mu = 0. \quad (24)$$

The structural sums can be evaluated if $h'(t)$ fluctuates either as a vector or a scalar. The vector variation is especially plausible when it is kept in mind that particles in shear flow have to avoid one another and therefore—in an ever-changing direction—they are closer together or further apart. The scalar variation is associated with a phenomenon of hole formation that has been observed in numerical simulations. More dense and less dense regions appear ephemerally whether there is shear or not. It is simply a property of slurry flow, see for example the two-dimensional simulations in Koenders *et al* (2012). To make progress the fluctuations $h'(t)$ —in a rather primitive assertion—are expressed as fractions of the average value as

$$\frac{h'^{\mu\nu}}{d}(t) = -s^\mu (a'^{\mu}(t) + b'_m{}^{\mu}(t) n_m^{\mu\nu}). \quad (25)$$

The averages $\langle a'^{\mu}(t) \rangle$ and $\langle \mathbf{b}'^{\mu} \rangle$ are obviously zero. The structural sums in equation (24) can now be evaluated using the expressions in (16); this leads to an estimate for $\mathbf{v}'^{\mu}(t)$

$$v_i'^{\mu}(t) = -\frac{d}{5} \left(b'_i{}^{\mu}(t) \alpha_{jk}^\mu + \frac{d}{2} a'^{\mu}(t) \alpha_{jkl}^\mu \right) (\delta_{ij}\delta_{kl} + \delta_{il}\delta_{kj} + \delta_{ik}\delta_{jl}) = 0. \quad (26)$$

In order to obtain an estimate for the local granular temperature \mathbf{v}'^{μ} is squared and then the time average will be taken; the latter, of course does *not* vanish, but yields a value. The average

will contain terms $\langle (a'^{\mu})^2 \rangle$, $\langle b'^{\mu}_q b'^{\mu}_r \rangle$ and $\langle a'^{\mu} b'^{\mu}_q \rangle$. A reasonable simplifying assumption that can be made is that over the averaging time, the direction of the vector \mathbf{b}'^{μ} is random. That would imply that $\langle a'^{\mu} b'^{\mu}_q \rangle$ is negligible and that $\langle b'^{\mu}_q b'^{\mu}_r \rangle$ contributes significantly only when $q = r$.

Implementing these ideas then, for transparency and compact presentation two auxiliary tensors are introduced

$$\hat{\alpha}'^{\mu}_{il} = \alpha'_{jk}{}^{\mu} (\delta_{ij}\delta_{kl} + \delta_{il}\delta_{kj} + \delta_{ik}\delta_{jl}); \quad \hat{\alpha}'^{\mu}_i = \alpha'_{jkl}{}^{\mu} (\delta_{ij}\delta_{kl} + \delta_{il}\delta_{kj} + \delta_{ik}\delta_{jl}). \quad (27)$$

Using these the local granular temperature takes the form

$$\langle v'^{\mu}_i(t) v'^{\mu}_i(t) \rangle = \frac{d^4}{100} (\hat{\alpha}'^{\mu}_i)^2 \langle (a'^{\mu})^2 \rangle + \frac{d^2}{25} \hat{\alpha}'^{\mu}_{iq} \hat{\alpha}'^{\mu}_{ir} \langle b'^{\mu}_q b'^{\mu}_r \rangle. \quad (28)$$

Following the notion that $\langle b'^{\mu}_q b'^{\mu}_r \rangle$ only has diagonal components that contribute significantly leads to an expression with two constants $\langle (a'^{\mu})^2 \rangle$ and $\langle (b'^{\mu}_r)^2 \rangle$

$$T^{\mu} = \langle v'^{\mu}_i(t) v'^{\mu}_i(t) \rangle = \frac{d^4}{100} (\hat{\alpha}'^{\mu}_i)^2 \langle (a'^{\mu})^2 \rangle + \frac{d^2}{25} \hat{\alpha}'^{\mu}_{iq} \hat{\alpha}'^{\mu}_{iq} \langle (b'^{\mu}_r)^2 \rangle. \quad (29)$$

Now the granular temperature T may be inserted into the expression for the particle pressure (9)

$$\bar{p} = \alpha_4 \frac{\eta}{d} \phi \frac{d}{h} \sqrt{\left(\frac{d^4}{100} (\hat{\alpha}'^{\mu}_i)^2 \langle (a'^{\mu})^2 \rangle + \frac{d^2}{25} \hat{\alpha}'^{\mu}_{iq} \hat{\alpha}'^{\mu}_{iq} \langle (b'^{\mu}_r)^2 \rangle \right)}. \quad (30)$$

For d/h the average value $1/s$ is used

In the literature a convenient expression for the relation between s and the solidosity ϕ is given (Torquato *et al* 1990),

$$\frac{1}{s} = \frac{12\phi(2-\phi)}{(1-\phi)^3}. \quad (31)$$

Plotting this functional relationship—figure 1—on a logarithmic scale, it is seen that a good power law fit in the range $0.2 < \phi < 0.6$ can be achieved, which works out as

$$\frac{1}{s} \approx 447\phi^{2.5}; \quad \phi \approx 0.087s^{-2/5}. \quad (32)$$

In many instances this may be quite a practical approximation. Note that s^{-1} is quite a steep function of the solidosity.

From the combination of N_c and the ϕ dependence of s as given by equation (31) the estimated viscosity follows through equation (23). This is used by Davis *et al* (2008) and it is found that for $N_c \approx 6$ a very good fit is obtained compared with experiments. In Guazzelli and Pouliquen (2018) a number of estimates is presented for the solidosity dependence of the shear viscosity. In passing it is noted that these do vary somewhat; typically, at the high end of the validity range that is of relevance in this paper ($0.2 < \phi < 0.6$) by some 30 percent.

Another measure for d/h is Bagnold's linear concentration (Bagnold 1954). Jenkins and Hanes (1998) mention this parameter and then relate it to Torquato *et al* (1990); the linear concentration and equation (31) are thus equivalent.

2.4. The rheology of \bar{p} , $\langle (a'^{\mu})^2 \rangle$, $\langle b'^{\mu}_q b'^{\mu}_r \rangle$

Although it is generally recognised that the particle pressure—and thereby the shear-induced migration process—is associated with fluctuations that necessarily take place in a flowing

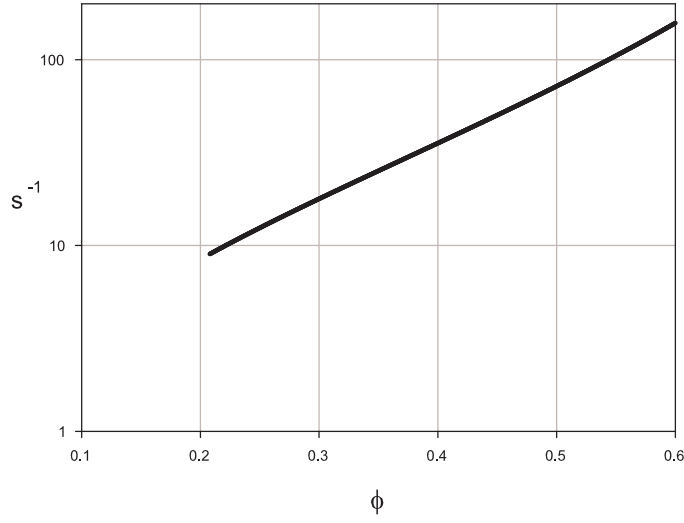


Figure 1. The functional relationship, equation (31), of d/h as a function of ϕ .

slurry, the partition of the fluctuations into a scalar and a vector part is the main focus of this paper. A rheology for these three parameters—pressure, scalar and vector decomposition—needs to be derived from experiments. They will depend of course on the local value of the solidosity; however a more global influence may be present as well. Furthermore, if the rheological sensitivity should contain a length scale, then, disappointingly, no obvious one comes to the fore. Thus, the rheology needs to be captured in power law expressions.

Starting point for the particle pressure is the expression (9). This expression accounts primarily for the *magnitude* of the force that gives rise to the particle pressure. More plausibility for this expression can be injected by making use of the analysis in the previous section. A special case is studied in which there is a shearing strain rate in two dimensions only; thus α_{12} is the only non-zero component of α and the double gradient is zero. This implies that $\langle (a'^{\mu})^2 \rangle$ is irrelevant and—in this special case only—is set to zero. It then follows from equation (26) that

$$\langle v'^2 \rangle^{\mu} = \frac{d^2}{25} \alpha_{12}^2 \langle b'^2 \rangle^{\mu} = \frac{d^2}{25} \alpha_{12}^2 \frac{\langle (h')^2 \rangle^{\mu}}{d^2} s^{-2}. \quad (33)$$

The coefficient of variation $\sqrt{\langle (h')^2 \rangle^{\mu} / d^2} / s$ may be related to the fraction of the space between the particles in which they ‘jitter’ to the average space available. The available space is approximately $\pi d^2 h / 4$ a variation is $\pi d^2 \sqrt{\langle (h')^2 \rangle} / 4$ and the ratio of the two is just the coefficient of variation. The probability of a solid contact event between two particles is plausibly proportional to this coefficient. This is a purely spatial argument that shows that \sqrt{T} is proportional to the probability of an encounter. What it does not deal with is the *number of encounters in the measurement time* τ , which is concerned with the frequency of the jitters. A measure for this would be the inverse of the time it takes to traverse the gap between particles, which is proportional to $1/s$.

These ideas inform how the coefficient in the expression for the particle pressure depends on the solidosity: a power factor is inserted into (9)

$$\bar{p} = \bar{\alpha}_4 \frac{\eta}{d} \phi \left(\frac{d}{h} \right)^{n_p} \frac{d}{h} \sqrt{T}. \quad (34)$$

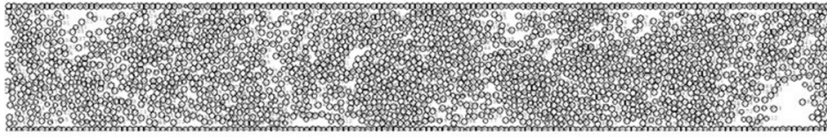


Figure 2. Image of a slurry flow in 2-d. Reproduced from Koenders *et al* (2012) with permission from the Royal Society of Chemistry. Note the fluctuations in the solidosity.

Below, experiments will provide some guidance as to what value for the exponent n_p is reasonable. However, it is expected—based on the hand-waving arguments given in the previous paragraph—that n_p is close to 1.

In order to understand the rheology of $\langle (a'^{\mu})^2 \rangle$ the distribution of fluctuations in a sheared slurry needs to be understood. Solidosity fluctuations may have any size and a flowing slurry exhibits a spectrum of fluctuations, which is both pervasive and persistent. These global solidosity fluctuations will somehow become manifest in the scalar parameter sensitivity, though at this stage it is difficult to say how exactly.

Parenthetically it is noted that the large-scale fluctuations (which are also the largest in magnitude) operate on a scale that is comparable to the size of the problem. These effects are clearly visible in a two-dimensional numerical simulation, see figure 2. It is immediately clear that these solidosity variations do not take place on the cell scale (one particle, surrounded by its immediate neighbours), but rather involve a substantial number of cells. Similarly, in the images produced by the simulations by Seto and Giusteri (2018) the variations are clearly visible.

The functional sensitivity of the coefficient $\langle b'^{\mu}_q b'^{\mu}_r \rangle$ is required. As noted above, the vector \mathbf{b}'^{μ} operates on the cell level. It can only depend on the local solidosity and in such a way that it is large when the excursions that particle μ needs to carry out take place in a very dense medium, while they will be smaller in a less densely packed slurry.

In this context it must be mentioned that the much-discussed jamming transition is generally not directly relevant to the problem to hand. When the solidosity reaches a critical maximum value, *enduring* contacts between the solid particles become evident. The jamming ‘transition’ has been studied quite extensively in the physics literature, for example Liu and Nagel (2010) (it is of special interest for physicists, as it is regarded as a phase transition) and in cooling magmas close to the maximum crystal packing fraction: Marsh (1996), Hoyos *et al* (2022) and Florez *et al* (2024).

Now, when there is a region in the flow where the solidosity is so large that jamming takes place, the surface-to-surface distance between particles is of the order of magnitude of the roughness scale of the constituents. This scale is small compared to the particle size (although in certain geophysical applications it may be of the same order of magnitude), but also small compared to the value of h in the mean flow. Because of the fluctuations in the problem a region of the flow that has a mean solidosity that is close to the jamming solidosity will exhibit some regions where the slurry is actually jammed and the fluctuations in the surface-to-surface distance lead to near-infinite values of d/h . The extent of these regions depends on the proximity of the mean solidosity in this region of the flow to the jamming solidosity. However, the mean solidosities in the current flow problems— $\phi \approx 0.2$ – 0.4 —are generally well below the jamming transition solidosity of $\phi \approx 0.6$. Also relatively smooth particle surfaces will be assumed with $\delta_r/d < 0.01$ typically.

The motion of the particles in a cell causes an evolution in the parameters a' and \mathbf{b}' . The change in $h^{\mu\nu}$ follows from $(\mathbf{v}'^\nu - \mathbf{v}'^\mu)\mathbf{n}^{\mu\nu}$. Estimates of the velocity fluctuations are available through expression (26). In lowest order the contribution from the surrounding particles (labelled ν) are neglected. The question is then how the motion of the central particle (labelled μ) affects a' and \mathbf{b}' . The influence on the vector parameter is quite easily ascertained by evaluating $\mathbf{v}'^\mu\mathbf{b}'^\mu$. Using expression (26) it follows

$$v_i'^\mu b_i'^\mu = \frac{d}{5} b_i'^\mu \left(b_i'^\mu(t) \alpha_{jk}^\mu + \frac{d}{2} a'^\mu(t) \alpha_{jkl}^\mu \right) (\delta_{ij}\delta_{kl} + \delta_{il}\delta_{kj} + \delta_{ik}\delta_{jl}). \quad (35)$$

Consider strain rate paths that are isotropically contracting, that is $\alpha_{jk} = \alpha\delta_{jk}$ ($\alpha < 0$, as these are generally associated with particles coming very close (the strain rate gradient is neglected for the moment)). Now it is seen that

$$v_i'^\mu b_i'^\mu = d\alpha (b'^\mu)^2. \quad (36)$$

Thus it follows that the velocity fluctuation opposes the vector \mathbf{b}' and therefore this vector will reduce in magnitude in a contraction. No such argument can be put forward for the scalar a'^μ , which in this lowest order approximation remains unchanged. The reduction in the magnitude of $(d/h)b'$ is especially pronounced when d/h is large. All in all then, it is expected that the rheology of $\langle b_q'^\mu b_r'^\mu \rangle$ is rather different than the one for the particle pressure and $\langle (a'^\mu)^2 \rangle$. The former involves no influence from the global solidosity fluctuations, while the latter will contain both global and local elements. As remarked above, experiment must be the guide.

It was noted in the introduction that one of the problems with the cell model and granular temperature model is the fact that the term in the temperature that is proportional to the strain rate is a—generally huge—factor $(W/d)^2$ greater than the term that is proportional to the strain rate gradient. The rheological dependence on power laws makes the problem very sensitive to the relevant exponents; this is exacerbated by the fact that all the coefficients appear as quadratic terms. So it is easy to see how two somewhat different exponents could lead to a substantial factor of $(d/h)^\epsilon$, which could easily balance $(W/d)^2$ if ϵ is of the order of $1 - 4$.

3. Form of the equations in conduit flow

The problem is treated in two dimensions. The flow is in the x -direction, propelled by a scaled external pressure gradient

$$G = \frac{40}{9\eta N_c} \frac{\partial p}{\partial x}. \quad (37)$$

d^2G has the dimension of a velocity. The mean velocity \mathbf{v} has an x -component: $v_1(y)$. Migration takes place in the y -direction; therefore the primary variables T , \bar{p} and ϕ are functions of y only and p does not depend on y . The balance equations take the form

$$\frac{\partial v_1}{\partial y} \frac{d}{h} = Gy + C + \int_0^y \phi(y) dy (\rho_f - \rho_s) g_1 \quad (38)$$

where C is an integration constant. It follows that the only non-vanishing components of α_{jk} and α_{jkl} are

$$\begin{aligned} \alpha_{12} = \hat{\alpha}_{12} &= s(Gy + C) + \int_0^y \phi(y) dy (\rho_f - \rho_s) g_1; \\ \alpha_{122} = \hat{\alpha}_{122} &= \frac{\partial}{\partial y} \left[\frac{h}{d} (Gy + C) \right] + \phi(y) (\rho_f - \rho_s) g_1. \end{aligned} \quad (39)$$

The other stress equilibrium equation is with $H = (\rho_s - \rho_f)g_2$

$$-\frac{\partial \bar{p}}{\partial y} + H\phi = 0 \rightarrow \frac{\partial}{\partial y} \left(\bar{\alpha}_4 \frac{\eta}{d} \phi s^{-n_p-1} \sqrt{T} \right) = H\phi \quad (40)$$

$$\rightarrow \bar{\alpha}_4 \frac{\eta}{d} \phi s^{-n_p-1} \sqrt{T} = H \int_0^y \phi(y) dy + D \quad (41)$$

where D is another integration constant with the dimension of a pressure.

Below a special case is studied in which the particles are neutrally buoyant ($\rho_f = \rho_s$); as a consequence—for this case $H = 0$. This situation is especially relevant when it comes to the comparison with experiment with symmetrical flow in a conduit. Another special case that pertains to horizontal flow in a conduit is also considered; for this case $g_1 = 0$.

s is a steep function of ϕ . There are two ways of dealing with ϕ in the front factor in equation (40). The first is to set the solidosity to an average $\bar{\phi}$, leaving a differential equation in $s(y)$. However, it is very easy to absorb $\phi(y)$ into $s(y)$ in equation (40), using the term $s(y)$ through (32). In the cases where $g_2 = 0$ the latter is used. The former is the preferred way forward where only a small range of values of ϕ is relevant.

The rheology is introduced as follows. For the particle pressure equation (34) is used. Similarly, for $\langle (b'_r)^\mu \rangle^2$ a local form is introduced: $\langle (b'_r)^\mu \rangle^2 = c_2 s^{-n_b}$. The form of $\langle (a'^\mu) \rangle^2$ contains both local and global influences and is unknown at this stage, but will be informed by experiment; for convenience the abbreviations

$$\langle (a'^\mu) \rangle^2 = c_1(s) \quad \text{and} \quad \langle (b'_r)^\mu \rangle^2 = c_2 s^{-n_b} \quad (42)$$

are employed. Using these forms and the expression for $\phi(y)$ as outlined above, the differential equation turns into

$$(0.087)^2 \bar{\alpha}_4^2 \frac{\eta^2}{d^2} s(y)^{-4/5} s(y)^{-2-2n_p} \left(c_1[s(y)] \frac{d^4}{100} (\hat{\alpha}'_t)^\mu + \frac{d^2}{25} \hat{\alpha}'_{iq} \hat{\alpha}'_{iq} c_2 s(y)^{-n_b} \right) \quad (43)$$

$$= \left(H \int_0^y \phi(y) dy + D \right)^2. \quad (44)$$

3.1. Symmetrical flow

For symmetrical flow, which is a situation that can be quite easily tested against experiments with neutrally buoyant particles, $H = 0$ and $C = 0$. The domain is $-W < y < W$; the length scales in the problem can be scaled to W , so that $y = \tilde{y}W$. Equation (43) takes the form

$$s(\tilde{y})^{-14/5-2n_p} \frac{(0.087)^2 \bar{\alpha}_4^2 \eta^2 d^2 G^2}{100} \left(c_1(s) \left[\frac{\partial}{\partial \tilde{y}} (s(\tilde{y}) \tilde{y}) \right]^2 + 4 \frac{W^2}{d^2} \tilde{y}^2 c_2 s^{2-n_b} \right) = D^2. \quad (45)$$

This would be easy enough to solve if only it was known what the functional form of $c_1(s)$ is. To find that out an experiment is interrogated. The paper by Frank *et al* (2003), is consulted. Here the solidosity profile in conduit flow is examined for various Peclet numbers. The one of interest in this case is the highest Peclet number, so Brownian motion is negligible. The migration is studied for particles with a diameter of $2 \mu\text{m}$ flowing through rectangular channels with a cross section of $50 \mu\text{m} \times 500 \mu\text{m}$; the ensuing solidosity profile is studied using confocal

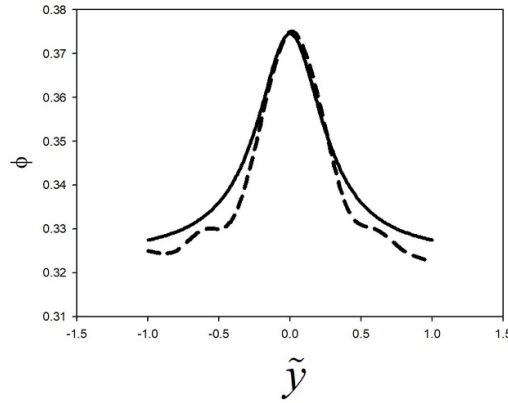


Figure 3. Dashed line: solidosity profile of a Brownian suspension from data as measured by Frank *et al* (2003) at $Pe = 4400$; solid line: fit according to equation (46).

microscopy. The experiments pertinent to this paper were carried out at a bulk solidosity of $\bar{\phi} = .34$.

In order to fit the findings by Frank *et al* (2003) to the experiments a simple rational approximation is employed, setting

$$s(\tilde{y}) = s_0 + \frac{A\tilde{y}^2}{1 + B\tilde{y}^2}. \quad (46)$$

A reasonable approximation of experiments is obtained for $A \approx 0.11$, $B \approx 9.6$ and $s_0 = 0.026$, see figure 3. The fit deviates somewhat from the tails in the experiment and is such that the ‘nose’ of the profile and the bulk solidosity are accurately represented. Substituting the fit (46) into the ruling differential equation and expressing the result back as a function of s gives c_1 as a function of s .

Before embarking on this exercise the behaviour of $s(\tilde{y})$ in the vicinity of $\tilde{y} = 0$ is investigated. To that end set $s(\tilde{y}) = s_0 + s_1\tilde{y}^2 + s_2\tilde{y}^4$ and substitute in the differential equation. It follows immediately that

$$D^2 = (0.0087)^2 \bar{\alpha}_4^2 \eta^2 d^2 G^2 \frac{c_1(s_0)}{s_0^{4/5+2n_p}}; \quad s_1 = 4 \frac{W^2}{d^2} \frac{c_2 s_0^{-n_b+2n_p+19/5}}{(2n_p - 16/5) c_1(s_0) - s_0 \left(\frac{\partial c_1}{\partial s} \right)_{s_0}}. \quad (47)$$

In passing it is noted that $s_1 = A$. From the experiments it is seen that $s_1 > 0$ and so it follows that if, say, in the vicinity of s_0 $c_1(s)$ behaves as $a_1 s^{-n_a}$, then the condition $n_p > 8/5 - n_a/2$ must be satisfied.

The scheme of implementing the fit (46) can now be implemented. First \tilde{y}^2 is expressed in terms of $s(\tilde{y})$. A simple inversion gives

$$\tilde{y}^2 = \frac{s - s_0}{B(s_0 - s) + A}. \quad (48)$$

For the values of s_0 , A and B as quoted above there are two points of particular interest. The first is the point at which $\tilde{y} = 1$, which yields $s \approx 0.036640$ and marks the end of the validity range of the current fit. The second is slightly beyond this point; the denominator vanishes—corresponding to $\tilde{y} \rightarrow \infty$ —at $s = 0.037746$. It is seen that these two value are very close to one another and as a result in the vicinity of $s \approx s(\tilde{y} = 1)$ the inversion is not very reliable. This must be kept in mind when the method is implemented.

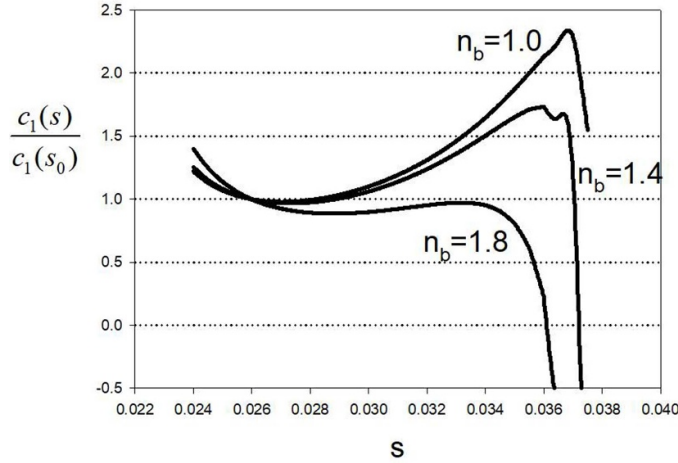


Figure 4. $c_1(s)/c_1(s_0)$ as a function of s for $n_p = 1.1$, $c_2^{(r)} = 0.01$ and various values of n_b . The irregularity near the peak for $n_b = 1.4$ is the result of a small numerical error.

Substituting (46) into the differential equation and applying the inversion (48) by straightforward algebra yields the following form for $c_1(s)$

$$\frac{c_1(s)}{c_1(s_0)} = A^2 \frac{(As_0^{-2np-4/5} + Bs_0^{1/5-2np})s^{2np+14/5} - Bs^{19/5+2np}s_0^{-2np-4/5} + c_2^{(r)}(s^{-nb+2}s_0 - s^{-nb+3})}{9(-2/3(s-s_0)^2 B + A(s-2/3s_0))^2 (A + (s_0 - s)B)} \quad (49)$$

$$\text{with } c_2^{(r)} = \frac{4W^2 c_2}{c_1(s_0) d^2}. \quad (50)$$

In order to obtain an impression of the shape of this function an order of magnitude of $c_2^{(r)}$ is needed. For the experiments to hand the front factor $4W^2/d^2 \approx 500$. $c_1(s_0)$ is the quadratic ratio of the scalar contribution to the fluctuations to the mean value of d/h at the densest point; it is of order unity or larger. The vector contribution of this same quantity is rather smaller due to the ameliorating evolution effect outlined in the section on the rheology of $\langle (b)^2 \rangle$ and may be of the order of 0.1 or even smaller. Thus $c_2 s^{-nb}$ on average is of the order of 0.1. Setting the average value of s to 0.03 it follows that $c_2^{(r)}$ is of the order of 0.05 if $n_b \approx 2$. These are obviously ballpark figures.

In figure 4 an illustrative set of plots is presented of the resulting values of $c_1(s)/c_1(s_0)$ as a function of s for various values of n_b . These plots show first of all that the outcome is highly dependent on the choice of parameters. Nevertheless, a pattern can be discerned that points to the underlying physics. At the low end of s , that is high solidosity, the behaviour of c_1 is exponential. At the high end of the graph peculiar things happen and these are entirely associated with the fact that the approximation (46) is inadequate for s greater than the limiting value. Inbetween these extremes the exponential behaviour for low s transitions to either a plateau or a slightly increasing behaviour of c_1 . This reflects the origin of the scalar intensity of the solidosity fluctuations. For large solidosities a local effect dominates, one that operates on the cell scale. For smaller solidosities the distribution of fluctuations at a larger scale is manifest. *In extremis* it could be argued that for small mean solidosities the quadratic fluctuation content

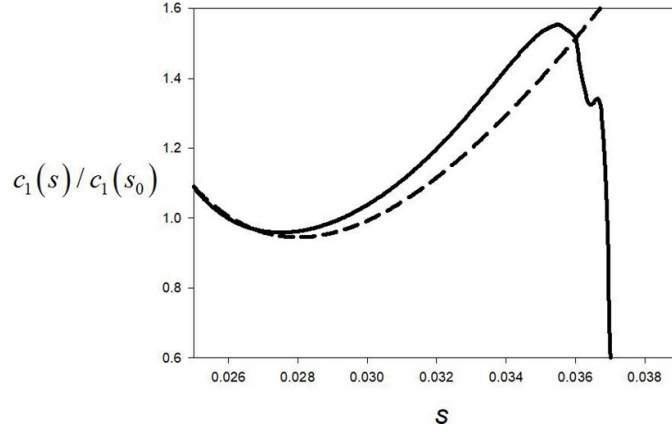


Figure 5. Solid line: $c_1(s)/c_1(s_0)$ as a function of s for $n_p = 1.1$, $c_2^{(r)} = 0.01$ and $n_b = 1.5$; dashed line: the estimate (52) for $a_a = -6$, $n_a = 3$ and $c_m \approx 1$ and $s_m \approx 0.027$. The slight irregularity post-peak is the result of a numerical error.

is independent of the solidosity, as these would be dominated by the large-scale effects, and therefore the ratio $(s')^{-2}/(s^{-1})^2$ (which is proportional to c_1) would behave proportional to s^ϵ , with $\epsilon = 2$. It does not go quite like that, as local effects ameliorate this dependence and—certainly at medium solidosities—the value of ϵ will be smaller. Looking at the graph, figure 5, $\epsilon \approx 1$ is not unreasonable.

Many more variations with different variables can be carried out—varying n_p , $c_2^{(r)}$, as well as n_b —however, the pattern displayed in figure 5 persists to a greater or lesser extent. This confirms the underlying physics, although it is not a simple theory.

It is now desirable to have a simple approximation for the behaviour of c_1 . Noting the exponential behaviour at small values of s and increasing tendency at larger s , the following is put forward

$$\frac{c_1}{c_1(s_0)} \approx A_a s^{-n_a} + a_a + s b_a. \quad (51)$$

The curve has a minimum at $c_1/c_1(s_0) = c_m$ for $s = s_m$ and using that the approximation in these terms becomes

$$\frac{c_1}{c_1(s_0)} \approx a_a - \frac{a_a - c_m}{n_a + 1} \left[\left(\frac{s}{s_m} \right)^{-n_a} + n_a \frac{s}{s_m} \right]. \quad (52)$$

This may be substituted into the differential equation and using $c_m \approx 1$ and $s_m \approx 0.027$ it is found that the value $B = 9.62$ is achieved for the combination $n_a = 3$ and $a_a \approx -6$ and requiring the approximation to give the correct result at $\tilde{y} = 0.8$. The latter has been chosen as a compromise between the fact that B comes into play for large values of \tilde{y} , but also that $\tilde{y} = 1$ is just where the fit to experiments (46) becomes inaccurate. In the graph, figure 5, the two approaches are shown: the approximation (52), which has few parameters and has validity beyond $s \approx 0.08$ and the result from fitting (46) directly to the differential equation.

While most of the effort so far has been on finding constitutive expressions to describe the experiments, it is now possible to investigate the sensitivity to other parameters as long as the solidosity is still operating in broadly the same range. One parameter that is easily changed is the channel width. Setting $(W/d)^2$ to twice the value as the one appropriate to Frank *et al*

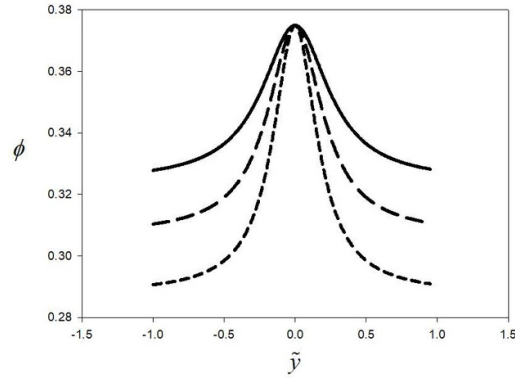


Figure 6. Solidosity profiles for various ratios of W^2/d^2 . Solid line: the situation as given by the approximation, equation (46), to Frank *et al* (2003) ($4W^2/d^2 \approx 500$), long dash: $4W^2/d^2 \approx 1000$, short dash: $4W^2/d^2 \approx 2000$.

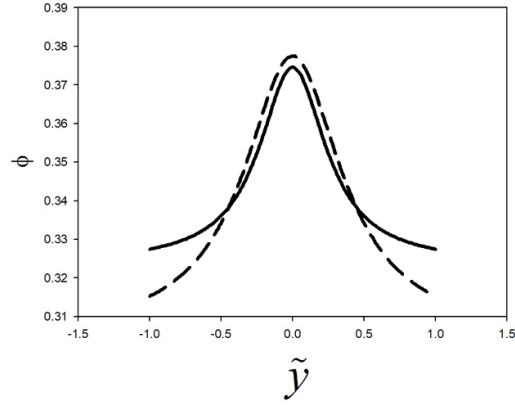


Figure 7. Solidosity profiles at constant bulk solids fraction for two ratios of W^2/d^2 . Solid line: the situation as presented by the approximation, equation (46), to Frank *et al* (2003) ($4W^2/d^2 \approx 500$), long dash: $4W^2/d^2 \approx 1000$.

(2003), the solidosity profile is established in the same approximation as before, that is by fitting the form (46) with A also increased by a factor of 2 (A is proportional to $(W/d)^2$). B is determined from the differential equation in the vicinity of $\tilde{y} = 0.8$. It follows that $B \approx 13$ and the ensuing solidosity profile is shown in figure 6. Increasing $(W/d)^2$ by another factor of 2 yields $B \approx 18$, again shown in figure 6. In this calculation s_0 has been kept constant, implying that $\bar{\phi}$ varies. Alternatively $\bar{\phi}$ may be kept constant, which leads to a rather more complicated (numerical) calculation. Essentially, equation (47) has to be integrated using (52) while s_0 is varied until the correct value of $\bar{\phi}$ is achieved ($\bar{\phi} = 0.34$). The result is shown in figure 7.

It is seen that a broader channel makes the profile relatively more sharply defined around the centre of the conduit; relatively, because the values of y are scaled to the conduit half-width. The value of the volume fraction at the tip of the nose is not much affected by the channel width.

3.2. Non-symmetrical flow

For non-symmetrical flow neither C nor D vanish. The asymmetry may be associated with the density contrast being non-zero, that is $H \neq 0$, or the boundary conditions being different at either side of the conduit. Scaling as before results in

$$\begin{aligned} c_1(s) \left\{ \frac{\partial}{\partial \tilde{y}} [s(\tilde{y})(\tilde{y} + \tilde{C})] \right\}^2 + 4 \frac{W^2}{d^2} [s(\tilde{y})(\tilde{y} + \tilde{C})]^2 c_2 s^{-n_b} \\ = \frac{100}{(0.087)^2 \bar{\alpha}_4^2 G^2 \eta^2 d^2} \left(WH \int_0^{\tilde{y}} \phi(\tilde{y}) d\tilde{y} + D \right)^2 s^{14/5+2n_p} \end{aligned} \quad (53)$$

where $\tilde{C} = C/(GW)$.

At the same time the velocity field is to be studied. From equation (38)

$$\frac{\partial v_1}{\partial y} \frac{d}{h} = Gy + C \rightarrow v_1(y) = \int_{-W}^y (Gy + C) s(y) dy + v_1(-W). \quad (54)$$

A special case of the non-symmetrical flow is one in which there are few solids and these are distributed in a thin layer on the side of one of the walls of the conduit. Depending on the sign of the density contrast this will be either the top or the bottom. Here the case of the latter is considered; the problem is then not dissimilar from the bed-loading problem; the difference is that the traditional bed-loading problem is usually studied in the context of a turbulent flow—see Jenkins and Hanes (1998), Raudviki (1998)—whereas here the flow is laminar due to the high viscosities of the fluids involved. The special case of a thin layer of solids at the bottom involves a large region with no particular content where the flow is dictated by the viscosity of the fluid η and the small region (with a thickness of a few particle diameters) where a dense slurry may be expected and which is ruled by the current granular temperature model. The latter needs some modification due to the presence of the solid boundary.

A procedure for the determination of the constant C is now put forward. It makes no sense to determine this constant from a boundary condition that is far away from the dense slurry and therefore boundary conditions at, or near, the bottom of the conduit must be considered. At the same time the flow at the bottom must be connected to the flow properties in the large region as this obviously drives the dense slurry flow. The boundary conditions that will be used at the bottom is the slipping boundary condition for the velocity and the temperature, see Chapman and Cowling (1970), Petford and Koenders (1998). This boundary condition reads

$$v_{bd} = \frac{2 - \theta}{\theta} \lambda \left. \frac{\partial v}{\partial y} \right|_{bd} \quad (55)$$

where the subscript bd refers to the boundary, θ is a constant, λ the mean free path and another constant. The idea behind this condition, which is relevant to gases, is that on collision with the wall a proportion of the particles θ is ‘caught’ in the interstices of the boundary (and thus it says something about the roughness of the wall) while the remainder is reflected elastically. Before the particles hit the boundary they have a velocity $\lambda \partial v / \partial y$ and thus there is a temperature jump as described by equation (55). While it is doubtful that such a relation for gases will hold exactly for dense slurries, its form certainly will be not unlike it. Note that if the mean free path is zero then the velocity at the wall must also be zero and that if no particles are captured, that is $\theta = 0$, then the velocity gradient must vanish.

In principle a numerical approach may now be used using the rheologies determined in the previous sections. Here, analytical insight is preferred and to that end it is advantageous to introduce a tentative form for the solidosity profile near the boundary. By way of a first

approach a simple two-parameter form is used, one to specify the solidosity at the boundary and another one indicating the extent of the thickness of the layer of solids

$$\phi(y) = \phi(-W) \exp^{-(W+y)/\Delta}. \quad (56)$$

The shape of this curve is suggested by the low-Shields number solution, that is the one closest to the laminar regime, in Jenkins and Hanes (1998). The extent of the layer at the bottom is small, so it may be assumed that $\Delta \ll W$. The total solids content may then be evaluated as

$$\int_{-W}^{\infty} \phi(-W) \exp^{-(W+y)/\Delta} dy = \Delta \phi(-W). \quad (57)$$

This will be a prescribed amount, corresponding to a mean solidosity $\bar{\phi}$, so $\Delta \phi(-W) = 2W\bar{\phi}$, which fixes $\phi(-W)$. Employing (32), furthermore, gives an approximation for $s(y)$

$$s(y) \approx \frac{0.0022}{\phi(-W)^{2.5}} \exp^{2.5(y+W)/\Delta}; \quad s(-W) \approx \frac{0.0022}{\phi(-W)^{2.5}}. \quad (58)$$

Next the attention is focussed on the determination of C . The connection between the flow in the conduit region—where there are no particles—and the flow in the region where the cumulant is located is established. The former region is ruled by the viscosity η . For conduit flow (width $2W$) it holds that the mean flow velocity $\langle v \rangle$ is related to the pressure gradient as

$$\frac{\partial p}{\partial x} = -\frac{3\eta \langle v \rangle}{W^2}. \quad (59)$$

The velocity of the fluid near the boundary a distance y_0 away from it ($y = -W + y_0$) is

$$v_f(y) = \frac{1}{2\eta} \frac{\partial p}{\partial x} (y^2 - W^2) \rightarrow v_f(y) = -\frac{1}{\eta} \frac{\partial p}{\partial x} W y_0. \quad (60)$$

From equation (54) the velocity of the particles is known, as long as the boundary condition is specified. For the moment a very rough boundary is assumed, so that $v_1(-W) \approx 0$, then

$$\begin{aligned} v_1(y) &= \frac{0.0022}{\phi(-W)^{2.5}} \\ &\times \left(0.4\Delta C - 0.16\Delta^2 G - 0.4\Delta G W - (0.4\Delta C - 0.16\Delta^2 G + 0.4\Delta G y) e^{2.5 \frac{y+W}{\Delta}} \right) \end{aligned} \quad (61)$$

The velocity of the particles and the velocity of the fluid are now assumed to be equal, so in the limit $\Delta \ll W, y_0 \ll W$ the condition for C becomes

$$\begin{aligned} \frac{C}{G} &\approx (0.4\Delta + W - y_0) \frac{e^{2.5y_0/\Delta}}{e^{2.5y_0/\Delta} - 1} - \frac{W}{e^{2.5y_0/\Delta} - 1} - \frac{\phi(-W)^{2.5}}{0.0022} \frac{0.5625 N_c W y_0}{\Delta (e^{2.5y_0/\Delta} - 1)} \\ &\rightarrow \frac{C}{G} \approx W - \frac{\phi(-W)^{2.5}}{0.0022} \frac{0.5625 N_c W y_0}{\Delta (e^{2.5y_0/\Delta} - 1)} = W \left[1 - f_{bd} \left(\phi(-W), \frac{y_0}{\Delta} \right) \right]. \end{aligned} \quad (62)$$

The evaluation of the second term on the right hand side involves some speculation; set $\phi(-W) \approx 0.4, N_c \approx 6$ then the function $f_{bd}(\phi(-W), y_0/\Delta)$ gives the correction to $C/G = W$. The function is plotted in a range $2 < y_0/\Delta < 5$, figure 8.

The question is then, what is a reasonable value for the ‘thickness’ of the boundary flow. Once a value is established, or estimated, C is known.

The behaviour of the granular temperature at the boundary is more problematic. The reason is that the temperature, the solidosity and the velocity are all continuum variables, but the

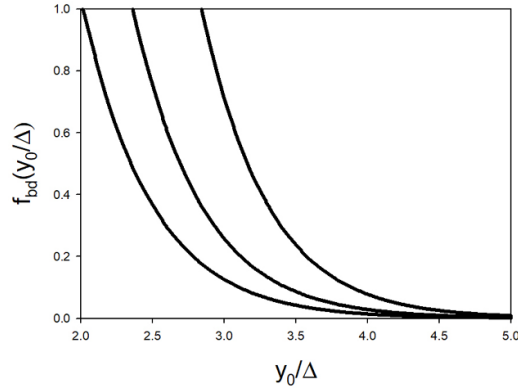


Figure 8. Sensitivity of the second term in equation (62) to $\phi(-W)$ and y_0/Δ .

distance between the particles and the relative velocity with which they approach, or depart from, each other very near the boundary is not a continuum property, as it involves individual particles. So, the continuum view and individual particle behaviour have to be reconciled. Starting point is the force balance equation (40), which reads

$$\frac{\partial}{\partial y} \left(\bar{\alpha}_4 \frac{\eta}{d} \phi \left(\frac{d}{h} \right)^{n_p} \frac{d}{h} \sqrt{T} \right) = \phi H; \rightarrow \bar{\alpha}_4 \frac{\eta}{d} \phi_b \frac{\partial}{\partial y} \left(s^{-n_p-1} \sqrt{T} \right) = \phi_b H. \quad (63)$$

Here, the continuum variable ϕ has been replaced by an average parameter ϕ_b that represents a mean over the first couple of particle diameters near the boundary. Now the boundary condition for the temperature needs to be imposed. Following Chapman and Cowling (1970) this boundary condition is similar to the one put forward in (55)

$$T_{bd} = \frac{2-\theta}{\theta} \lambda \left| \frac{\partial T}{\partial y} \right|_{bd}. \quad (64)$$

Developing (63) gives

$$\begin{aligned} \bar{\alpha}_4 \frac{\eta}{d} \frac{\partial}{\partial y} \left(s^{-n_p-1} \sqrt{T} \right) &= H; \\ \rightarrow \bar{\alpha}_4 \frac{\eta}{d} \left[(-n_p-1) s^{-n_p-2} \frac{\partial s}{\partial y} \sqrt{T} + s^{-n_p-1} \frac{\partial T}{\partial y} \frac{1}{2\sqrt{T}} \right] &= H. \end{aligned} \quad (65)$$

The field variable T is a continuum variable that gives an average over the first few particle diameters near the boundary, but is here merely used to impose the boundary condition (64); the result is

$$\bar{\alpha}_4 \frac{\eta}{d} \left[(-n_p-1) s^{-n_p-2} \frac{\partial s}{\partial y} \sqrt{T} + s^{-n_p-1} \frac{\theta}{2\lambda(2-\theta)} \sqrt{T} \right] = H. \quad (66)$$

At this point the temperature may be replaced by its average field value T_{bd} , leaving a differential equation in $s(y)$, which describes the relative distance between the particle surfaces in the first layer near the boundary, but which is not a continuum variable. The solution for the differential equation is

$$s(y) = \left[\frac{2\lambda Hd(2-\theta)}{\bar{\alpha}_4 \eta \theta \sqrt{T_{bd}}} + c \text{nst} \exp \left(-\frac{\theta y}{2\lambda(2-\theta)} \right) \right]^{-1/(n_p+1)}. \quad (67)$$

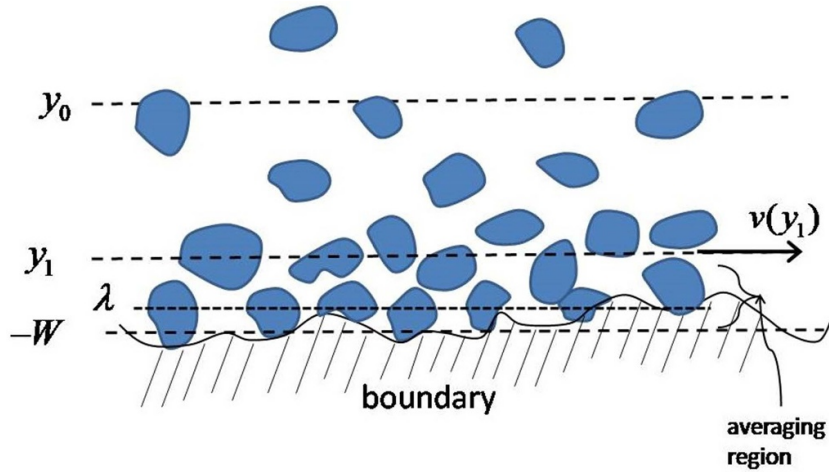


Figure 9. A sketch to give an impression of the set up and the various length scales.

The temperature in the boundary region needs to be estimated. The role of the temperature in this context is to describe the speeds with which particles approach or depart to and from each other. The particles in the boundary are supposed to lie still, so the speed that needs to be estimated is that of the first layer, which is at a distance y_1 from the particles at the bottom: $y_1 \approx 2d$. A sketch that gives an impression of the set-up is presented in figure 9.

From the velocity gradient it follows that

$$v(y_1) = \left(\frac{\partial v}{\partial y} \right)_{y=-W} y_1 = s(-WG - C)y_1 = -sWGf_{bd}y_1 \quad (68)$$

$$\text{with } f_{bd} = 1 + \frac{C}{WG}. \quad (69)$$

From the solution (67) it is seen that the critical parameter for the distance from the boundary is the mean free path λ . This parameter is likely to be of the order of magnitude of the surface to surface distance between neighbouring particles, so $\lambda \ll d$, in fact λ is of the order of $h = sd$. A solidosity dependence need to be introduced as well, because the denser the medium the more likely it is that particles will collide; thus, as a first estimate $\lambda \propto \phi_b^{-1}$. This implies that the exponential term in (67) becomes negligible once y has moved to a distance of a particle diameter away from the boundary, which is the beginning of the region where continuum variables begin to make sense.

The temperature at the boundary is associated with the velocity difference between the particles at $y = y_1$ and those at $y = y_b = y(-W)$; the latter are considered to lie still. Hence, just above the first moving layer, where $y \approx y_1$, it holds that

$$s(y_1) \approx \left[\frac{2\lambda Hd(2-\theta)}{\bar{\alpha}_4 \eta \theta \sqrt{T_{bd}}} \right]^{-1/(n_p+1)}, \quad \text{with } \sqrt{T_{bd}} \approx |v(y_1)| = |sWGf_{bd}y_1|. \quad (70)$$

Solving for H yields

$$H = \frac{20}{3} \frac{\bar{\alpha}_4 \eta f_{bd} \theta}{N_c (2-\theta)} \frac{y_1}{\lambda d} s(y_1)^{-n_p} \frac{\langle v \rangle}{W} \quad (71)$$

where $G = 40/(9\eta N_c)(\partial p/\partial x)$ and $\partial p/\partial x = -3\eta\langle v \rangle W^2$ were used.

It is seen that for an equilibrium to materialise the density contrast H must be proportional to a macroscopic shear rate $\langle v \rangle/W$. Now, identify $s(y_1)$ with $s(-W)$, $\phi_b = \phi(-W)$, $y_1 \approx 2d$ and set the mean free path as $\lambda \approx 2s(-W)d/\phi_b$ and a condition for Δ emerges

$$H = \frac{40}{3} \frac{\bar{\alpha}_4 \eta f_{bd} \theta}{N_c (2 - \theta)} \frac{s(-W)^{-n_p - 1}}{\Delta} \bar{\phi} \frac{\langle v \rangle}{d}. \quad (72)$$

This has transformed the condition from one phrased in terms of ϕ_b and $\langle v \rangle/W$ to one that depends on the mean solidosity $\bar{\phi}$ and the shear gradient per particle $\langle v \rangle/d$. Using then equation (58) and the preferred value of $n_p = 1.1$, the condition reads

$$H = 1.9 \times 10^8 \frac{\bar{\alpha}_4 \eta f_{bd} \theta}{N_c (2 - \theta)} \frac{1}{\Delta} \left(\frac{\Delta}{W \bar{\phi}} \right)^{-21/4} \frac{\langle v \rangle}{d}. \quad (73)$$

Note that $WL\bar{\phi}$ represents the total volume of solids per unit breadth and unit length in the conduit. These solids will be concentrated near the lower boundary, forming a cumulate layer. The value of Δ is most easily represented as a multiple of the grainsize: $n_\Delta = \Delta/d$.

In evaluating the result it is noted that the group of parameters $1.9 \times 10^8 \bar{\alpha}_4 \eta f_{bd} \theta / [N_c (2 - \theta)] \langle v \rangle$ operates as one block. Below the values of all these are fixed, except $\langle v \rangle$, as in varying this one, implicitly variations in the other ones are also studied. The other parameter variations pertain to $\bar{\phi}$ and d .

The results, which are meant to illustrate the sensitivity to various parameter variations, are plotted in figure 10. Note that the parameters used are relevant to geophysical applications that have a high value for the viscosity, ensuring laminar flows.

From the figure it is seen that the thickness of the cumulate decreases with increasing density contrast, while the solidosity at the boundary increases with increasing density contrast (the physically realistic range of $\phi(-W) < 0.65$ is investigated). This is obviously as expected: the cumulate is more compressed as the density contrast is larger. Furthermore the figure demonstrates the opposite effect to the density contrast as the parameters involved in the particle pressure are varied, or when the total available solids volume is modified. The choice of the parameters has been such that they are in a plausible geological range.

It is noted that for this analysis no value of D had to be evaluated, as all the relevant physics is represented in the analysis of the boundary conditions. D may be obtained by studying a case well beyond the boundary, for example at a distance $y = -W + \Delta$ using the rheology parameters as established in the previous sections. Because all the insights in the formation of the cumulate are already evident from the boundary conditions analysis, no explicit calculation of D is presented here (D will depend on Δ and also on all the other parameters that define the flow).

4. Conclusions

For dense suspensions particles in a flow field need to be able to make excursions around their mean flow path. These lead to fluctuations in the distance between the particles, which in turn may cause a particle pressure. The intensity of the fluctuations is the key parameter, which is known as the ‘granular temperature’. Using methods of granular mechanics this intensity may consist of a part due to an asymmetry in the fabric—the vector part—and a part due to the scalar variations in the fabric, which are local volume fraction variations. It transpires that

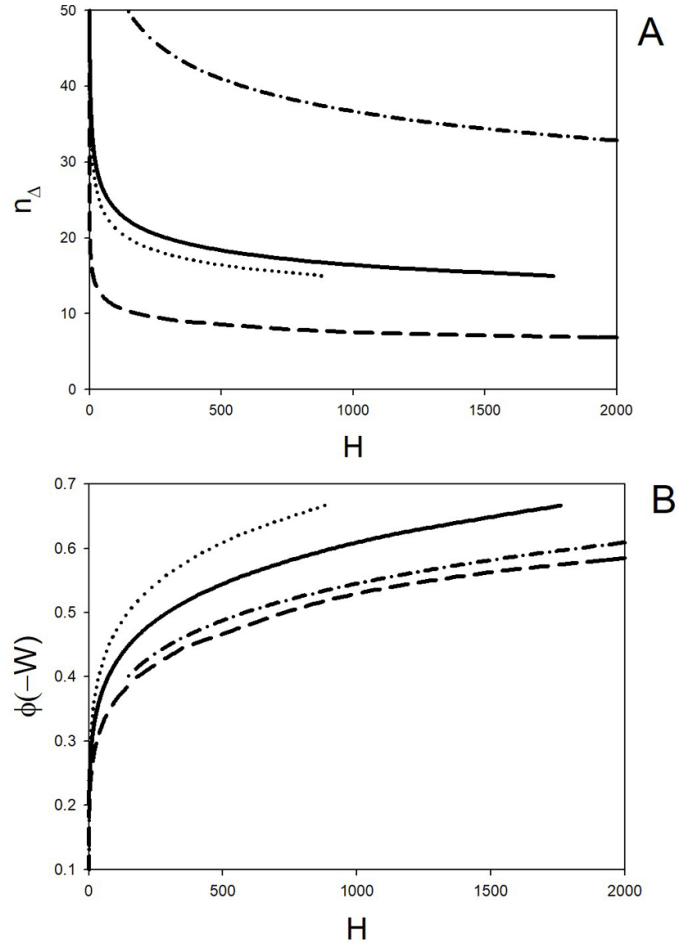


Figure 10. (A) Measure of cumulate thickness $n_{\Delta} = \Delta/d$ as a function of the mass density contrast $H = (\rho_s - \rho_f)g_2$ for various cases. (B) Solidosity at the bottom of the cumulate as a function of the density contrast. Parameters are: $\bar{\alpha}_4 = 0.004$, $\eta = 1.0$ Pa s, $f_{bd} = 0.1$, $\theta = 0.8$, $N_c = 6$. Solid lines: $\langle v \rangle = 0.1$ m s $^{-1}$, $d = 0.01$ m, $\bar{\phi} = 0.05$; dashed lines: $\langle v \rangle = 0.1$ m s $^{-1}$, $d = 0.01$ m, $\bar{\phi} = 0.02$; dotted lines: $\langle v \rangle = 0.05$ m s $^{-1}$, $d = 0.01$ m, $\bar{\phi} = 0.05$; dash-dotted lines: $\langle v \rangle = 0.1$ m s $^{-1}$, $d = 0.005$ m, $\bar{\phi} = 0.05$.

the former couples to the first gradient of the flow rate and the latter is associated with the double gradient. Rheologies for these two contributions to the fluctuation intensity, which is a time-averaged measure, are put forward and are further informed by experiments by Frank *et al* (2003). The elements of the granular temperature that pertain to the ‘energy balance’ as put forward by McTigue and Jenkins (1992) are not needed. For symmetrical flow in a conduit it is then possible to calculate the solidosity profile under various flow conditions and conduit dimensions. Using the double gradient avoids having an unphysical sharp peak in the profile that plagues theories that depend solely on the first gradient of the flow rate field.

For asymmetrical flow a special case is studied: a thin layer of solids by the side of the conduit. In order to maintain analytical insight an exponentially declining solidosity field is postulated. For these situations of dense slurries near a boundary slipping boundary conditions must be introduced. The thickness of the sediment layer may be determined under various flow and boundary conditions; a further parameter of interest is the mass density contrast, which has implications for geological resource exploration in magmatic systems, e.g. Barnes and Robertson (2019). The results are indicative and many refinements to the theory are possible. Induced anisotropy is one of them. Particle shape is also an unexplored area that is worthy of further study. For heterodisperse particle content, segregation is a worthwhile field of investigation. To study these and other interactions further, numerical simulations would be an appropriate tool, building on the analytical results presented here.

References

- Allgood C, Llewellyn E W, Humphreys M C S, Mathias S A, Brown R J and Vye-Brown C 2024 *J. Geophys. Res.: Solid Earth* **129** e2023JB028007
- Bagnold R 1954 *Proc. R. Soc. A* **225** 49–63
- Barnes S and Robertson J 2019 *Geosci. Front.* **10** 77–87
- Becker E and Buerger W 1975 *Kontinuumsmechanik* (Teubner)
- Bhattacharji S 1967 *J. Geol.* **75** 101–12
- Carlo L, Sarno L, Papa M N, Tai Y C and Villani P 2019 *Adv. Powder Technol.* **30** 2379–95
- Chapman S and Cowling T G 1970 *The Mathematical Theory of Non-Uniform Gases* 3rd edn (Cambridge University Press)
- Davis M, Koenders M A and Vahid S 2008 *Proc. Inst. Mech. Eng. C* **222** 1995–2006
- Dean E T R 2015 *Geotech. Res.* **2** 3–34
- Delannay R, Louge M, Richard P, Taberlet N and Valance A 2007 *Nat. Mater.* **6** 99–108
- Drew D A 1986 *Advances in Multiphase Flow and Related Problems* ed G Papanicolau (SIAM) pp 55–66
- Florez D, Huber C, Hoyos S, Pec M, Parmentier E M, Connolly J A and Hirth G 2024 *J. Geophys. Res.: Solid Earth* **129** e2024JB029077
- Frank M, Anderson D, Weeks E R and Morris J F 2003 *J. Fluid Mech.* **493** 363–78
- Gibb F 1968 *Geol. Mag.* **128** 51–66
- Guazzelli E and Pouliquen O 2018 *J. Fluid Mech.* **852** 1–73
- Gundogdu O, Koenders M A, Wakeman R J and Wu P 2003 *Chem. Eng. Sci.* **58** 10127–34
- Houlsby G 1981 Study of plasticity theories and their applicability to soils *Doctoral Thesis* University of Cambridge
- Hoyos S, Florez D, Pec M and Huber C 2022 *Geophys. Res. Lett.* **49** e2022GL100040
- Jenkins J T and Hanes D 1998 *J. Fluid Mech.* **370** 29–52
- Jenkins J T and Savage S B 1983 *J. Fluid Mech.* **130** 187–202
- Jenkins J and Koenders M A 2005 *Granular Matter* **7** 13–18
- Kim S and Karilla S J 1991 *Microhydrodynamics* (Butterworth-Heinemann)
- Koenders M A C 2020 *The Physics of the Deformation of Densely Packed Granular Materials* (World Scientific Publishing Europe Ltd)
- Koenders M A, Ibrahim M and Vahid S 2012 *Discrete Particle Modelling of Particulate Media* ed C-Y Wu (Royal Society of Chemistry) pp 39–45
- Koh C J, Hookham P and Leal L G 1994 *J. Fluid Mech.* **266** 1–32
- Komar P 1972 *Geol. Soc. Am. Bull.* **83** 3443–8
- Leighton D and Acrivos A 1987 *J. Fluid Mech.* **181** 415–39
- Li Y, Xu Q, Huang R, Chang C, Chen J and Wang Y 2024 *Geophys. Res. Lett.* **51** e2023GL104410
- Liu A J and Nagel S R 2010 *Annu. Rev. Condens. Matter Phys.* **1** 347–69
- Love A E H 1934 *A Treatise on the Mathematical Theory of Elasticity* 4th edn (Cambridge University Press)
- Lyon M K and Leal L G 1998 *J. Fluid Mech.* **363** 25–56
- Marsh D B 1996 *Min. Mag.* **60** 5–40

- McTigue D E and Jenkins J T 1992 *Advances in Micromechanics of Granular Materials* ed H H Shen (Elsevier Science) pp 381–90
- Miller R M and Morris J J 2006 *J. Non-Newtonian Fluid Mech.* **135** 149–65
- Nott P R and Brady J F 1994 *J. Fluid Mech.* **275** 157–99
- Petford N and Koenders M A 1998 *J. Geol. Soc.* **155** 873–81
- Phillips R J, Armstrong R C, Brown R A, Graham A L and Abbott J R 1992 *Phys. Fluids A* **4** 30–40
- Raudviki A 1998 *Loose Boundary Hydraulics* (Balkema)
- Seto R and Giusteri G G 2018 *J. Fluid Mech.* **857** 200–15
- Torquato S, Lu B and Rubinstein J 1990 *Phys. Rev. A* **41** 2059–74